

# Metal Foil Detectors assembly for the beam and background monitoring in the LHCb experiment<sup>1</sup>

---

V. Pugatch,<sup>a,2</sup> F. Alessio,<sup>b</sup> V. Balagura,<sup>c</sup> F. Blanc,<sup>d</sup> S. Chernyshenko,<sup>a</sup> V. Dobishuk,<sup>a</sup>  
V. Kyva,<sup>a</sup> O. Okhrimenko,<sup>a</sup> D. Ramazanov,<sup>a</sup> H. Schindler,<sup>b</sup> and O. Schneider<sup>d</sup>

<sup>a</sup>HEP Department, Institute for Nuclear Research of the NAS of Ukraine,  
47, Prospekt Nauky, 03028 Kyiv, Ukraine

<sup>b</sup>EP Department, European Organization for Nuclear Research (CERN),  
Genève 23, 1211 Geneva, Switzerland

<sup>c</sup>Laboratoire Leprince-Ringuet, CNRS/IN2P3, Ecole Polytechnique, Institut Polytechnique de Paris,  
Av. Chasles, 91120 Palaiseau, France

<sup>d</sup>High Energy Physics Laboratory, Ecole Polytechnique Fédérale de Lausanne (EPFL),  
BSP - Cubotron, 1015 Lausanne, Switzerland

E-mail: [pugatch@kinr.kiev.ua](mailto:pugatch@kinr.kiev.ua)

**ABSTRACT:** After an upgrade in 2019–2021, the LHCb experiment is taking data in Run 3 (2022–2026) with an instantaneous luminosity of proton-proton collisions of  $2 \times 10^{33} \text{ cm}^{-2} \text{ s}^{-1}$ . This article presents the Radiation Monitoring System (RMS-R3) for controlling the beam and background conditions at LHCb. It runs continuously during the detector's operation, and independently of the main LHCb data acquisition. Its design is based on robust and radiation-hard Metal Foil Detector technology. The RMS-R3 monitors the instantaneous luminosity and its evolution. The analysis of the RMS-R3 Run 3 data demonstrates its linear response with a high reproducibility in a five-decade dynamic range of luminosity over a long period of operation.

**KEYWORDS:** Beam-line instrumentation, Hardware and accelerator control systems, Radiation-hard detectors, Radiation-induced secondary-electron emission

---

<sup>1</sup>This document is the results of the research project funded by the EURIZON project, which is funded by the European Union under grant agreement No.871072. Grant #3014.

<sup>2</sup>Corresponding author.

---

## Contents

<b>1</b>	<b>Introduction</b>	<b>1</b>
<b>2</b>	<b>The LHCb experiment</b>	<b>2</b>
2.1	The LHCb detector	2
2.2	Beam and background monitoring systems	3
<b>3</b>	<b>The RMS-R3 Metal Foil Detectors assembly</b>	<b>4</b>
<b>4</b>	<b>Real-time luminosity monitoring and performance of RMS-R3</b>	<b>8</b>
<b>5</b>	<b>Conclusions and outlook</b>	<b>11</b>

---

## 1 Introduction

The LHCb experiment is primarily aimed at accurately measuring  $CP$  violation in the decays of particles with heavy quarks. Their unprecedented statistics accumulated at LHCb during Run 1 (2010–2012) and Run 2 (2015–2018) allowed to perform many important measurements related to the Cabibbo-Kobayashi-Maskawa matrix, responsible for  $CP$  violation in the Standard Model. LHCb also plays a significant and unique role in the studies of the lepton flavour universality, rare decays and the searches for processes beyond the Standard Model [1, 2].

The masses of charm and beauty quarks are relatively low compared to the LHC energies, and have low transverse momenta. The studied particles are most often produced close to the beams with a lot of background. Therefore, the LHC sets the number of interactions per bunch-crossing at LHCb much lower than in the ATLAS and CMS detectors, which target heavy particles like Higgs bosons. However, upgrading LHCb in 2019–2021 to cutting-edge technologies in triggering and event reconstruction allowed an increase in the number of interactions per bunch crossing from about one to five. After the commissioning period, the target luminosity of  $2 \times 10^{33} \text{ cm}^{-2} \text{ s}^{-1}$  has been reached in 2024 continuous running, 5 times higher than in Run 2. This should allow even more accurate measurements required for constraining various theoretical models [2, 3].

Another unique feature of the LHCb experiment is the ability to carry out studies of quark-gluon plasma simultaneously in two extreme regions of the QCD phase diagram: at high temperature—low density in collider mode, and high density—low temperature in fixed-target mode. The latter is achieved by injecting a tiny amount of gas into the beam pipe. The injection system, called SMOG, was also replaced in 2019–2021, and the new upgraded SMOG2 system [4] allowed to reach 100 times higher gas density than in Run 2.

The increased instantaneous luminosity requires special measures for the safety and efficiency of data taking. To ensure the successful operation of the LHCb detector, its Beam and Background monitoring systems were also upgraded. They include the new online luminometer PLUME, the

Beam Condition Monitors dumping the LHC beams in case of high backgrounds, and the Radiation Monitoring System (RMS-R3). The design and operation of the latter is the subject of this paper.

The RMS-R3 design is based on the technology of radiation hard Metal Foil Detectors (MFD) [5]. The signals of the eight MFDs are measured independently of the main LHCb data acquisition and other subdetectors. After calibration, they provide a measurement of the luminosity. A similar value is measured by the main luminometer PLUME, and is sent to the LHC. During PLUME downtime, the RMS-R3 luminosity takes over. The PLUME–RMS-R3 tandem ensures that the LHC can steer the beams such that the rate of the interactions per bunch-crossing is kept at the optimal level, which is crucial for the successful detector operation, and prevents excessive irradiation and ageing of the LHCb components.

## 2 The LHCb experiment

### 2.1 The LHCb detector

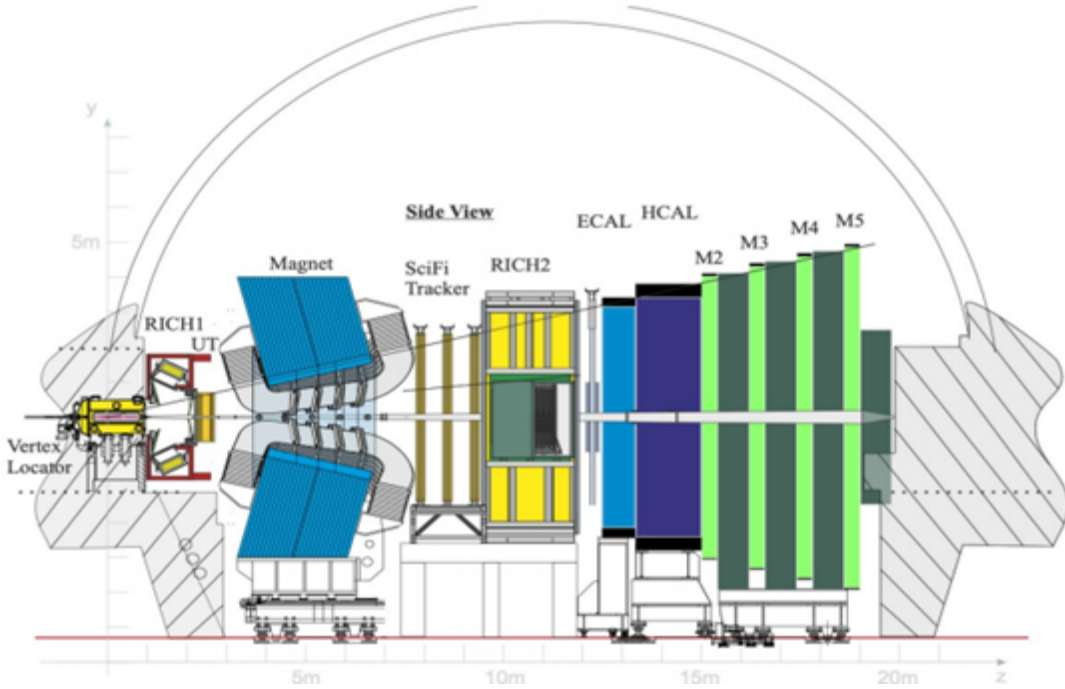


**Figure 1.** The scheme of the LHCb detector complex after Upgrade I in 2019–2021 (copied from [3]). The LHCb coordinate system is defined with the origin at the interaction point, with the  $z$  and  $y$  axes pointing to the right and upwards, respectively, while the  $x$  axis points into the figure plane making the system right-handed. According to the LHC convention, the beam codirectional (opposite) to the  $z$  axis is called beam one (two).

The LHCb detector [3, 6, 7] is a single-arm forward spectrometer covering the pseudorapidity range  $2 < \eta < 5$  (Figure 1). The detector has been substantially upgraded prior to the Run 3 data-taking period, in order to match the performance of the Run 1–2 detector, while allowing it to operate at approximately five times increased luminosity [3]. The high-precision tracking system has been fully replaced and consists of a silicon-pixel vertex detector surrounding the interaction region [8],

a large-area silicon-strip detector [9] located upstream of a dipole magnet with a bending power of about 4 T m, and three stations of scintillating-fibre detectors [9]. Different types of charged hadrons are distinguished using information from two ring-imaging Cherenkov detectors [10, 11]. The whole photon detection system of the Cherenkov detectors has been renewed for the upgraded detector. Photons, electrons and hadrons are identified by a calorimeter system consisting of electromagnetic and hadronic calorimeters. Muons are identified by a system composed of alternating layers of iron and multiwire proportional chambers [12]. Readout of all detectors into an all-software trigger [13] is a central feature of the upgraded detector, facilitating the reconstruction of events at the maximum LHC interaction rate, and their selection in real time. The trigger system is implemented in two stages: a first inclusive stage based primarily on charged particle reconstruction which reduces the data volume by roughly a factor of 20, and a second stage, which performs the full offline-quality reconstruction and selection of physics signatures. A large disk buffer is placed between these stages to hold the data while the real-time alignment and calibration is being performed.

## 2.2 Beam and background monitoring systems

Stable operation during the Run 3 period (2022–2026) in a harsh radiation environment created by hadron collisions in the LHCb interaction region requires continuous online monitoring of the beam-related conditions, particularly the instantaneous luminosity, the collision patterns of the LHC beams and the beam-induced background levels. The system should rapidly react and report any anomalies and abrupt changes of the running conditions.

New technical requirements for the online monitoring systems at LHCb were redefined for Run 3 and resulted in the construction of three independent systems: PLUME, BCM and RMS-R3, briefly presented below. All of them are integrated into the central control system of the LHCb experiment.

**PLUME** (Probe for LUMinosity MEasurement) [14, 15] is a new detector system specially developed for measuring the instantaneous luminosity in real time. In the PLUME luminometer, installed upstream of LHCb, 48 photomultipliers count Cherenkov light photons created in quartz radiators. The detector reports online both the total instantaneous luminosity at LHCb and the luminosity per bunch-crossing.

**BCM** (Beam Conditions Monitor) [3, 16] is a key safety system of the LHCb experiment, which performs fast control of the radiation levels induced by the LHC beams. It consists of 16 poly-crystalline chemical vapour deposited (pCVD) diamond pad sensors. They are installed on both sides of the interaction point and read out every 40  $\mu$ s. If the combination of the signals accumulated in any 80 or 1280  $\mu$ s time intervals exceeds the predefined thresholds, the system triggers the LHC beam dumps. This guarantees the safe operation and protection of the entire LHCb detector complex. The system operated successfully in Run 1–2. During Upgrade I, the sensors have been replaced, together with the support structures and electronics.

**RMS-R3** (Radiation Monitoring System for Run 3) [17] is a Metal Foil Detectors assembly consisting of four modules mounted 2.2 m upstream of the interaction point on the reinforced concrete wall separating the LHCb cavern from the LHC tunnel. They are installed in a top-bottom and left-right orientation with respect to the beam pipe, as shown in Figure 2. The system measures the LHCb instantaneous luminosity together with PLUME.

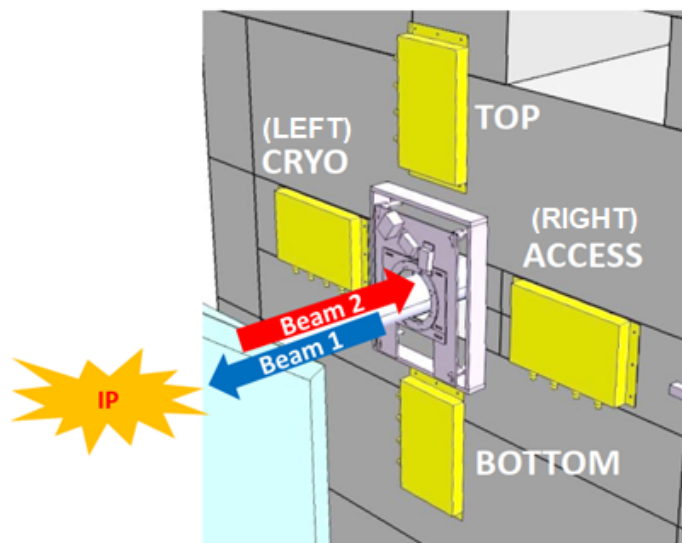


**Figure 2.** The layout of four RMS-R3 detector modules, each with two sensors. “Cryo” and “Access” denote the left and right module pairs when viewed from the LHCb cavern.

### 3 The RMS-R3 Metal Foil Detectors assembly

Radiation Monitoring Systems based on the MFD [5] technology are well established. They have been successfully running in various experiments: in the LHCb Inner Tracker [18–23] during Run 1–2 (2009–2018), as a luminosity monitor in the HERA-B experiment [24–26], and as almost “transparent” beam profile monitors at MPIfK (Tandem generator, Heidelberg) [25, 26] and CERN (SPS test line, Geneva, Switzerland) [23].

The RMS-R3 geometry layout (Figure 2) was designed to provide the monitoring of the LHCb beam and background. For reliability, the MFD sensors are duplicated in each module (Fig 3). The final positions of the ones nearest to the beam are chosen for having up to 300 kHz signal rate at the nominal LHCb luminosity of  $2 \times 10^{33} \text{ cm}^{-2} \text{ s}^{-1}$ . This should provide, on the one hand,  $\sim 0.1\%$  statistical accuracy of the frequency measurement and, on the other hand, a linear response to the instantaneous luminosity. The non-linearity is expected to appear at 1.3 MHz due to detector readout electronics. The distances from the beam axis to the centres of the two  $9 \times 9 \text{ cm}^2$  sensors in each module are 345 and 465 mm. The installation on the wall was performed with submillimeter accuracy by the technical support group at LHCb using the metrology methods developed at CERN.

One MFD detector together with the electrical connections is shown schematically in the bottom of Figure 4. The five-layer structure mounted on the printed circuit board has the sensor in the centre, two electrodes collecting secondary emitted electrons on both sides and two shielding layers. Charged particles hitting the  $9 \times 9 \text{ cm}^2$ ,  $50 \mu\text{m}$  thick copper foil in the centre generate secondary electron emission (SEE) [27, 28]. The induced positive charge is read out by a charge-to-frequency converter VFC110, sensitive at femto-Coulomb level. It has a stable voltage source to provide the baseline frequency and has a linear response in the input current range from 10 fA to 20 nA. The top and bottom shields, made of  $20 \mu\text{m}$  copper foils, ensure stable operation in high electromagnetic and radiation fields. The impact of environmental conditions, like temperature, humidity etc., on

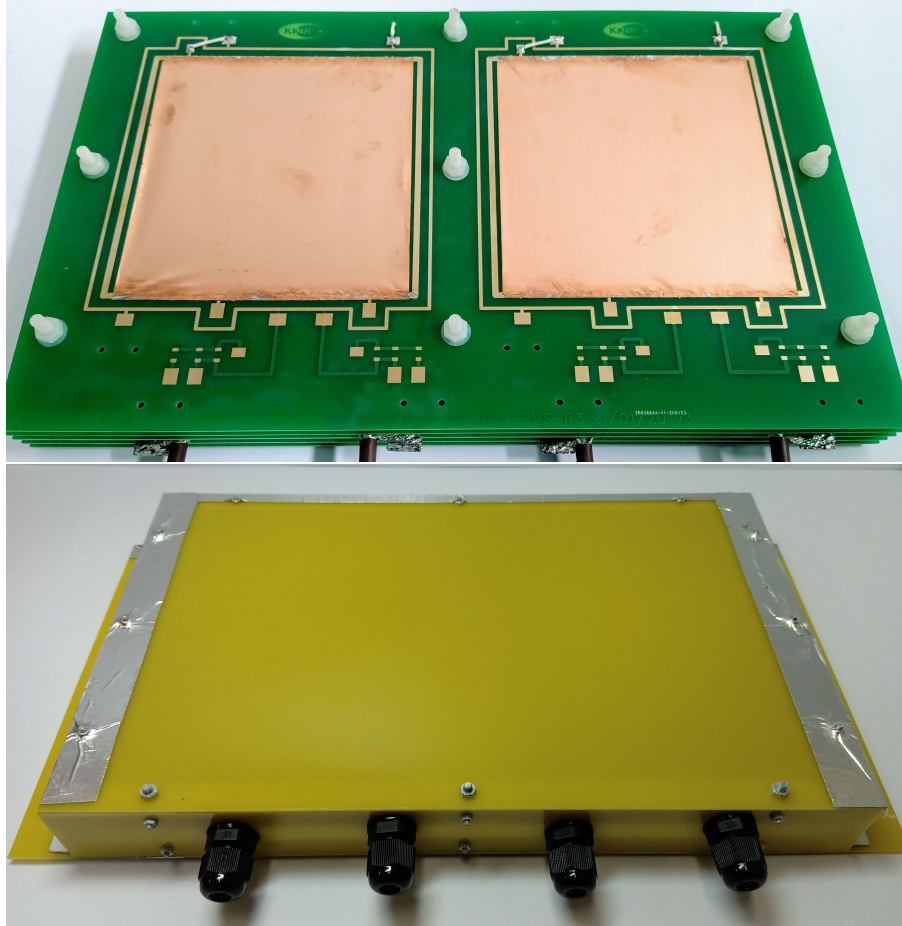


**Figure 3.** Photos of the detector module. The top one shows two sensors mounted on a single PCB with protective rings and contact pads for soldering BNC connectors. The bottom photo is taken after mounting the detector inside its metal case but before covering it with the protective aluminium foil. Two BNC connectors supply the bias voltage to the collecting electrodes, and the other two read out the sensor signals, as shown in Figure 4 (bottom plot).

the operational characteristics is minimized. The printed circuit boards are 1 mm thick and are made of FR-4 glass fiber with  $56\ \mu\text{m}$  copper tracks and pads. The contact elements are covered using ENIG-RoHS (Ni + Au) method. Special protective rings surround the sensor foils and electrodes and isolate them from potential surface cross-talk currents. The surface-mounted elements of RC filters are soldered on the collecting electrode panels. They filter out high-frequency noise picked up by the power lines.

The chosen module design has the advantage of providing sufficient mechanical rigidity, stable electrical contacts and relatively easy manufacturing and mounting.

Detector modules are assembled using polyamide bolts, nuts and washers in a housing made of G10-type material (glass textolite impregnated with an epoxy-phenolic connector), and covered with a thin aluminium foil. This provides both mechanical protection and electromagnetic shielding. Figure 3 shows a photo of the detector module without and with protective housing. All construction materials of the RMS-R3 detector modules were chosen following the safety rules in the LHC



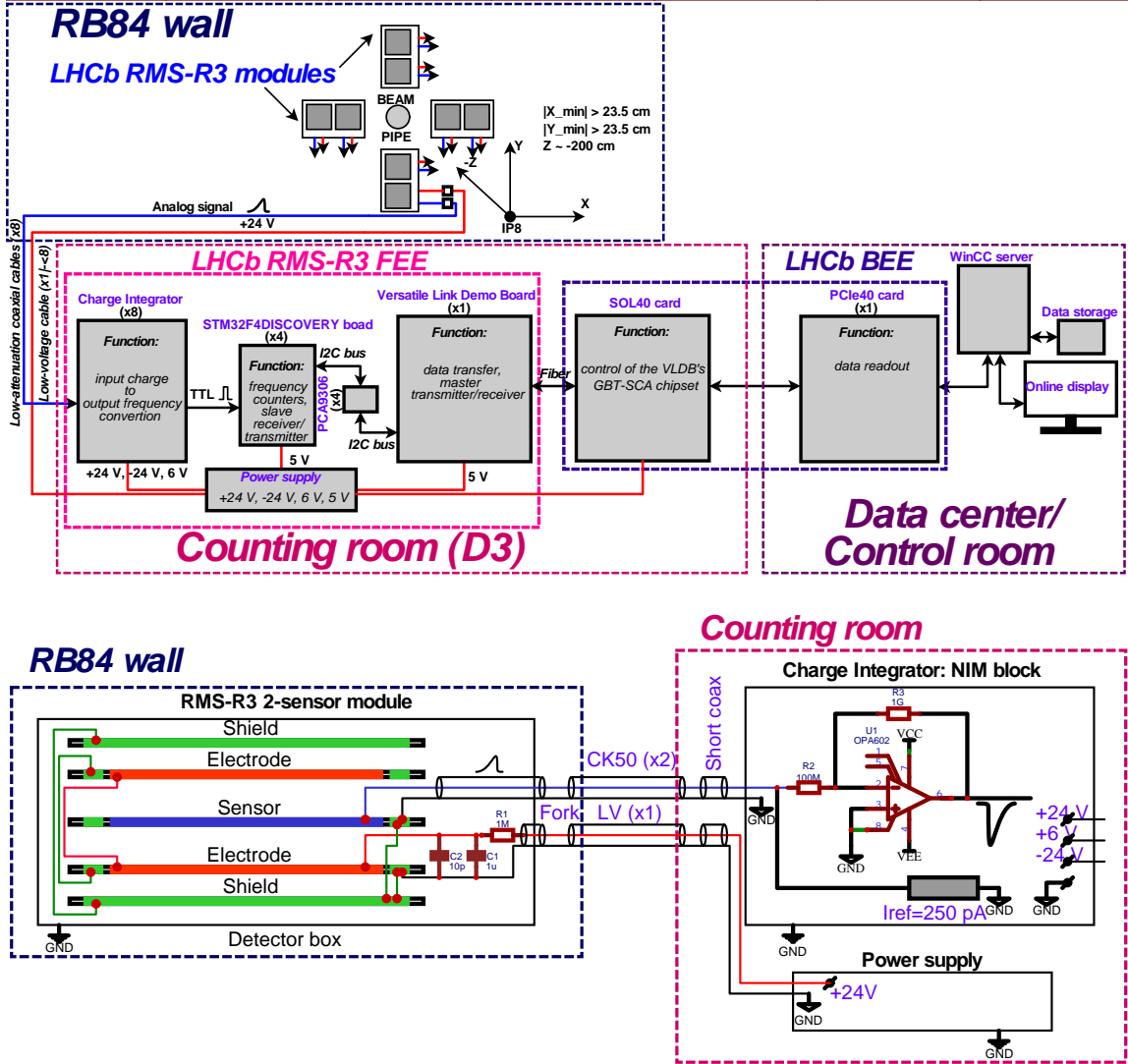


**Figure 4.** Top panel: schematic block diagram of the RMS-R3 detector modules. Middle panel: schematic block diagram of the Front-End-Electronics (FEE), with the devices in the counting room D3 shown on the left. Bottom left panel: detailed scheme of the RMS-R3 detectors mounted on the RB84 wall, illustrating the structure of a single detector module. Bottom right panel: counting room located at a 100 m distance away from the detector modules, connected by special cables to highly sensitive electronics.

experimental halls.

The SEE current increases with the positive voltage bias applied between the sensor and collecting electrodes, until it reaches a saturation plateau, as shown in Figure 5. It was obtained by irradiating a pair of MFD modules with a  $^{90}\text{Sr}$  beta-source. The saturation is reached at  $\sim 15 \text{ V}$ , while the RMS-R3 is operated at 24 V. The response stays constant up to 80 V.

Using a  $^{90}\text{Sr}$  beta-source at CERN, the calibration factor between the MFD output frequency and the number of particles hitting its area was determined to be  $550 \pm 180 \text{ particles/sensor/Hz}$ , where the 33% error is dominated by the 30% uncertainty of the beta-source activity. This and other parameters of the RMS-R3 modules are summarized in Table 1.

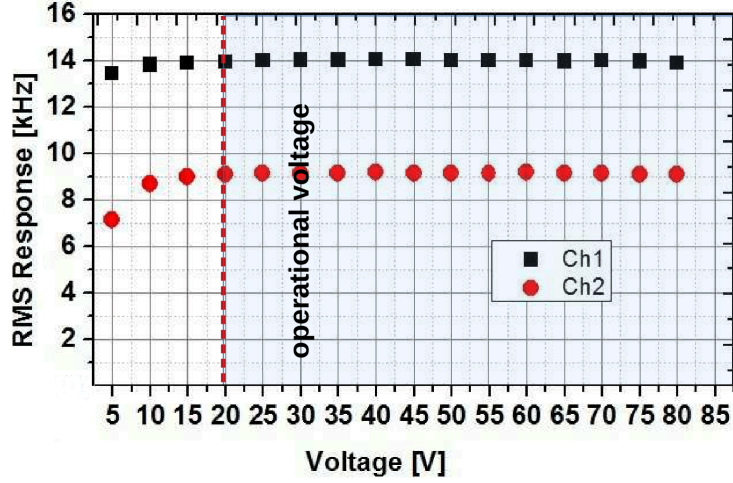


**Figure 5.** The response frequency of a pair of MFD sensors irradiated with a  $^{90}\text{Sr}$  beta-source as a function of the voltage applied between the sensor and collecting electrodes. The dashed vertical line at 20 V shows the minimal operational voltage. The RMS-R3 sensors work at 24 V.

**Table 1.** The main characteristics of the RMS-R3 modules. The MFD are well-known for their radiation tolerance, they easily withstand the harshest radiation levels in the LHCb environment. The frequency response of the sensor to one incident particle was measured with a  $^{90}\text{Sr}$  beta-source as explained in the text.

Parameter	Value
sensor	$9 \times 9 \text{ cm}^2 \times 50 \text{ }\mu\text{m}$ ( $0.1 X_0$ ) Cu foil
operational voltage	24 V
sensor-electrode capacity	25 pF
radiation hardness	$\approx 1 \text{ GGy}$ , $\approx 10^{20} \text{ MIP/cm}^2$
calibration	$10^3 \times$ expected at LHCb in Run 3
	$550 \pm 180 \text{ MIP/sensor/Hz}$

The schematic block diagram of the electronics and the readout lines of the RMS-R3 detector modules are presented in the bottom right and middle panels of Figure 4. As shown in the bottom, the sensor foils in the grounded modules are connected by low attenuation cables to the highly sensitive charge integrators mounted in the NIM crate in the counting room D3, located at 100 m distance. The charge integrator has a built-in Voltage–Frequency Converter (VFC) and a highly stable current source (250 pA) providing permanent calibration. The middle panel represents the front-end and back-end electronics on the left and right sides, respectively. The former consists of the Charge Integrator, STM32-F4DISCOVERY 32-bit counters [29], the Versatile Link Demo communication board (VLDB), and the PCIe40 SOL Card for ECS control [3, 30], all mounted in the LHCb counting room D3. The recorded values are transmitted by the VLDB and PCIe40 boards using 7-bit packets of the I<sup>2</sup>C protocol. The back-end electronics includes the PCIe40 Card, WinCC system (SCADA) from Siemens [31, 32], the data storage in the data centre and the displays



located in the LHCb Control Room.

The RMS-R3 online monitors present the instantaneous values and the evolution of the luminosity, together with all main parameters of the detectors: their signal frequencies, the bias voltages, and the status of the system components. The data are archived for further reference.

In each charge integrator, its internal 250 pA stable current source generates a constant 20–25 kHz baseline output. This is done to continuously check the operating conditions of all eight channels of the RMS-R3 system. After three years of operation, the baseline was stable within 0.5%, and its noise did not exceed 20 Hz, i.e. 0.02% of the nominal maximal response frequency of 300 kHz.

#### 4 Real-time luminosity monitoring and performance of RMS-R3

The absolute luminosity measurements at LHCb are described in Refs. [33, 34]. For any quantity  $f$  proportional to the instantaneous luminosity  $\mathcal{L}_{inst}$ ,

$$\mathcal{L}_{inst} = Af,$$

the proportionality coefficient  $A$  can be determined using the van der Meer calibration method [35]. To illustrate the idea, let's consider the collision of two bunches with  $N_{1,2}$  particles and  $\rho_{1,2}$  transverse densities moving in opposite directions, and denote by  $\mathcal{L}^{BX}$  the integrated luminosity per bunch-crossing. Then, the corresponding instantaneous luminosity is

$$\mathcal{L}_{inst}^{BX} = \mathcal{L}^{BX} f_{LHC} = Af^{BX}, \quad (4.1)$$

where  $f_{LHC} = 11.245$  kHz is the LHC bunch revolution frequency and  $f^{BX}$  is the rate induced only by the given bunch crossing. On the other hand, by the definition of the integrated luminosity,

$$\mathcal{L}^{BX} = N_1 N_2 \iint \rho_1(x, y) \rho_2(x, y) dx dy.$$

If the first bunch is separated by  $-\Delta x, -\Delta y$  in the transverse plane, the integral over  $\Delta x, \Delta y$  of this luminosity normalized by the number of particles is

$$\iint \frac{\mathcal{L}^{BX}(\Delta x, \Delta y)}{N_1 N_2} d\Delta x d\Delta y = \iint \rho_1(x_2 + \Delta x, y_2 + \Delta y) \rho_2(x_2, y_2) dx_2 dy_2 d\Delta x d\Delta y = 1, \quad (4.2)$$

where  $x_2, y_2$  are the coordinates of the stationary second beam. This can be easily seen by introducing new independent variables  $x_1 = x_2 + \Delta x, y_1 = y_2 + \Delta y$  which decouple the integrals  $\iint \rho_1(x_1, y_1) dx_1 dy_1$  and  $\iint \rho_2(x_2, y_2) dx_2 dy_2$ . The latter are equal to unity due to the normalization of  $\rho_{1,2}$ .

Using Eqs. 4.1 and 4.2 one gets the calibration factor

$$A = \left( \iint \frac{f^{BX}(\Delta x, \Delta y)}{f_{LHC} N_1 N_2} d\Delta x d\Delta y \right)^{-1} = \left( \iint r_{sp}^{BX} d\Delta x d\Delta y \right)^{-1}$$

by measuring  $f^{BX}(\Delta x, \Delta y)$  in  $\Delta x, \Delta y$  separation scans. Here,

$$r_{sp}^{BX} = \frac{f^{BX}}{f_{LHC} N_1 N_2}$$

is the normalized or “specific” rate ratio.

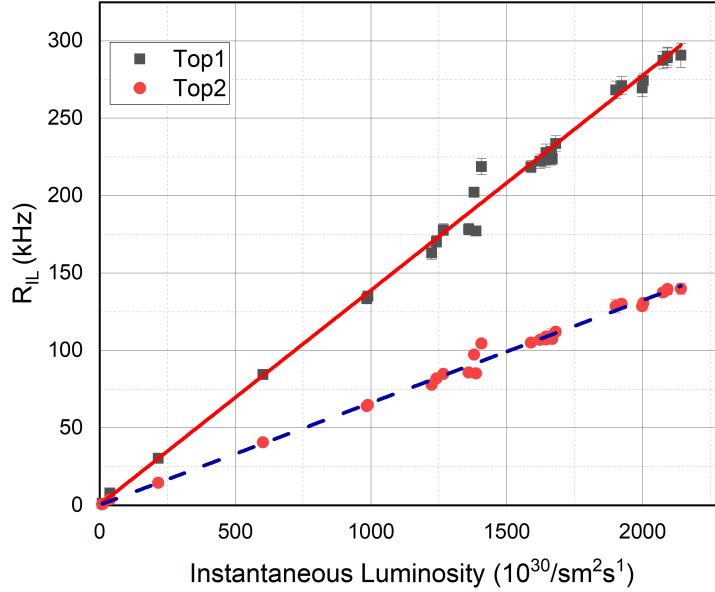
If the bunch densities are factorizable into  $x$  and  $y$  independent parts,  $\rho_{1,2}(x, y) = \rho_{1,2}^x(x) \cdot \rho_{1,2}^y(y)$ , the two-dimensional scan can be reduced to two one-dimensional scans, with only horizontal or vertical beam separations. In this case,

$$A = \left( \frac{\int r_{sp}^{BX}(\Delta x, \Delta y_0) d\Delta x \times \int r_{sp}^{BX}(\Delta x_0, \Delta y) d\Delta y}{r_{sp}^{BX}(\Delta x_0, \Delta y_0)} \right)^{-1}. \quad (4.3)$$

The values  $r_{sp}^{BX}(\Delta x, \Delta y_0)$  and  $r_{sp}^{BX}(\Delta x_0, \Delta y)$  with constant  $\Delta y_0$  and  $\Delta x_0$ , respectively, are measured in the horizontal and vertical beam separation scans, while  $r_{sp}^{BX}(\Delta x_0, \Delta y_0)$  in the denominator is obtained at the intersection of the  $x$  and  $y$  scan axes. See Ref. [36] for the proof of Eq. 4.3 and more details on van der Meer method.

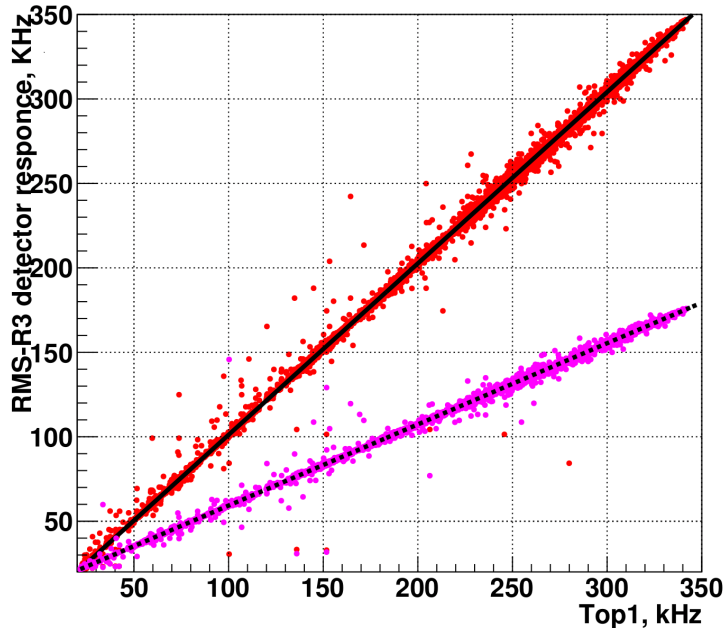
In practice, the absolute calibration factor in Eq. 4.3 was obtained at LHCb in van der Meer scans for PLUME luminometer, distinguishing the bunches, while RMS-R3 signals, integrated over all bunches, were recalibrated with respect to PLUME.

Figure 6 demonstrates the linearity of the RMS-R3 response with respect to the instantaneous luminosity measured by PLUME in proton-proton collisions recorded in 2024. The two lines correspond to two sensors in the “Top” module, the one closer to the beam has higher frequencies. The correlations in other RMS-R3 modules are similar.



**Figure 6.** The upper (lower) set of points shows the output frequency  $R_{IL}$  in kHz of the RMS-R3 “Top” sensor closer to (farther from) the beam versus the instantaneous luminosity measured by PLUME, in proton-proton collision data in 2024. The solid (dashed) lines represent the linear fits.

The bottom line in Figure 7 shows the linearity of the “Top” sensor responses with respect to each other. The upper line correlates the closest to the beam sensors in the “Top” and “Bottom” modules. For other pairs of sensors, the correlations are also similar.



**Figure 7.** The upper (lower) set of points shows the correlation between the frequencies measured in the closest to the beam sensors in the “Bottom” and “Top” RMS-R3 modules (the farthest and closest sensors in the “Top” module). The lines represent the results of the linear fit: slope = 1.015 and offset = 0.13 (slope = 0.481, offset = -0.03), where the offsets are calculated after a constant baseline subtraction.

This demonstrates the RMS-R3 capability to deliver high-precision real-time luminosity monitoring over a wide dynamic range. The reproducibility of the measurements across multiple sensing points confirms the robustness of the design and the reliability of the system for long-term operation. The high degree of stability observed over extended periods allows RMS-R3 to provide continuous and accurate information on radiation conditions in the LHCb interaction region, which is crucial for the beam and background monitoring.

The time evolution of the luminosities measured by RMS-R3 and the main online luminometer PLUME during one fill as an example is shown in Figure 8. Such plots are always available in the LHCb control room online.

The calibrated luminosity provided by the PLUME–RMS-R3 tandem is used by the LHC to keep the LHCb luminosity at the optimal level. When the LHC declares “stable beams” and the detectors are allowed to take data, the beam intensities in the beginning are high. Therefore, the LHC slightly separates the beams at LHCb. Then, due to the continuous loss of particles, mainly because of the interactions in the four LHC experiments, the beams get closer, and at the end of long runs collide head-on. This procedure is called the luminosity-leveling and is fully automated. It ensures the maximal event rate which can be accepted by the LHCb experiment. The complementarity and redundancy of the PLUME and RMS-R3 luminosity measurements ensure the accuracy and 100% availability of the luminosity values in real-time, which guarantees that the LHCb detector always works in the optimal conditions and takes good quality data.

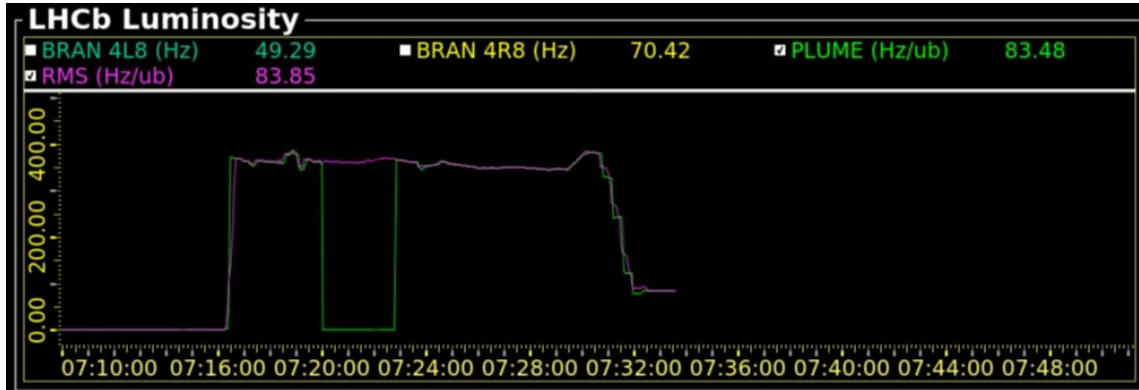


**Figure 8.** An example of the time evolution of the instantaneous luminosity measured by RMS-R3 and the main online luminometer PLUME, shown by the purple and green lines, respectively. In the period of PLUME downtime, when its values drop to zero, RMS-R3 takes over and becomes the main luminometer of LHCb.

## 5 Conclusions and outlook

The RMS-R3 detector assembly provides an autonomous real-time measurement of the instantaneous luminosity in the LHCb experiment during Run 3. RMS-R3 data demonstrate its linear response with high reproducibility in a five-decade dynamic range of instantaneous luminosity over a long period of operation. The Metal Foil Detector technology of the RMS-R3 is promising for any radiation-hard application like the monitoring of the beam, background and safety conditions in high energy physics experiments. The MFD detectors can withstand extreme levels of radiation expected at HL-LHC and future colliders like FCC, and are well suited for the luminosity measurements.

## Acknowledgments

The RMS-R3 monitoring system was implemented at the LHCb experiment (CERN, Geneva) by collaborators of the teams from the Institute for Nuclear Research of the National Academy of Sciences of Ukraine together with colleagues from CERN.

This project has received funding through the EURIZON project, which is funded by the European Union under grant agreement No.871072. Grant #3014.

## References

- [1] LHCb collaboration, *Implications of LHCb measurements and future prospects*, *Eur. Phys. J. C* **73** (2013) 2373 LHCb-PUB-2012-006, LHCb-PAPER-2012-031, CERN-PH-EP-2012-334, [1208.3355].
- [2] LHCb COLLABORATION collaboration, *Future physics potential of LHCb*, Tech. Rep. LHCb-PUB-2022-012, CERN-LHCb-PUB-2022-012, CERN, Geneva (2022).
- [3] LHCb collaboration, *The LHCb Upgrade I*, *JINST* **19** (2024) P05065 LHCb-DP-2022-002, [2305.10515].
- [4] LHCb COLLABORATION collaboration, *LHCb SMOG Upgrade*, Tech. Rep. CERN-LHCC-2019-005, CERN, Geneva (2019), DOI.

- [5] V. Pugatch, V. Aushev, C. Bauer, K. Knöpfle, M. Schmelling, M. Tkatch et al., *Metal foil detectors and their applications*, *Nucl. Instrum. and Methods in Phys. Res. A* **535** (2004) 566.
- [6] LHC<sub>B</sub> collaboration, *The LHC<sub>B</sub> detector at the LHC*, *JINST* **3** (2008) S08005.
- [7] LHC<sub>B</sub> collaboration, *LHC<sub>B</sub> detector performance*, *Int. J. Mod. Phys. A* **30** (2015) 1530022  
LHC<sub>B</sub>-DP-2014-002, CERN-PH-EP-2014-290, [[1412.6352](#)].
- [8] LHC<sub>B</sub> collaboration, *LHC<sub>B</sub> VELO Upgrade Technical Design Report*, Tech. Rep. CERN-LHCC-2013-021, CERN, Geneva (2013).
- [9] LHC<sub>B</sub> collaboration, *LHC<sub>B</sub> Tracker Upgrade Technical Design Report*, Tech. Rep. CERN-LHCC-2014-001, CERN, Geneva (2014).
- [10] M. Adinolfi et al., *Performance of the LHC<sub>B</sub> RICH detector at the LHC*, *Eur. Phys. J. C* **73** (2013) 2431 LHC<sub>B</sub>-DP-2012-003, [[1211.6759](#)].
- [11] LHC<sub>B</sub> collaboration, *LHC<sub>B</sub> PID Upgrade Technical Design Report*, Tech. Rep. CERN-LHCC-2013-022, CERN, Geneva (2013).
- [12] A.A. Alves Jr. et al., *Performance of the LHC<sub>B</sub> muon system*, *JINST* **8** (2013) P02022  
LHC<sub>B</sub>-DP-2012-002, [[1211.1346](#)].
- [13] LHC<sub>B</sub> collaboration, *LHC<sub>B</sub> Trigger and Online Upgrade Technical Design Report*, Tech. Rep. CERN-LHCC-2014-016, CERN, Geneva (2014).
- [14] LHC<sub>B</sub> collaboration, *LHC<sub>B</sub> PLUME: Probe for Luminosity Measurement*, Tech. Rep. CERN-LHCC-2021-002, LHC<sub>B</sub>-TDR-022, CERN, Geneva (2021), [DOI](#).
- [15] S. Barsuk, L. Roy, J. Rochet, G. Panshin, F. Sanders, V. Balagura et al., *Probe for Luminosity Measurement in LHC<sub>B</sub>*, Tech. Rep. LHC<sub>B</sub>-PUB-2020-008, CERN-LHC<sub>B</sub>-PUB-2020-008, CERN, Geneva (2020).
- [16] C. Ilgner, M. Lieng, M. Domke, M. Nedos, J. Sauerbrey, S. Schleich et al., *The Beam Conditions Monitor of the LHC<sub>B</sub> Experiment*, Tech. Rep. <https://cds.cern.ch/record/1233669>, CERN, Geneva (2010).
- [17] S. Chernyshenko, V. Dobishuk and V. Pugatch, *Functionality features of the RMS-R3 system in the third physics run of the LHC<sub>B</sub> experiment*, *Nuclear Physics and Atomic Energy* **25** (2024) 188.
- [18] M. Agari, C. Bauer, J. Blouw, W. Hofmann, S. Löchner, F. Maciuc et al., *Radiation Monitoring System for the LHC<sub>B</sub> Inner Tracker*, Tech. Rep. LHC<sub>B</sub>-2007-062, CERN-LHC<sub>B</sub>-2007-062, CERN, Geneva (2007).
- [19] V. Pugatch, Y. Pylypchenko, O. Okhrimenko, V. Iakovenko, V. Kyva, M. Borysova et al., *Radiation Monitoring System for LHC<sub>B</sub> Inner Tracker*, *Ukrainian Journal of Physics* **54** (2009) 418.
- [20] O. Okhrimenko, S. Barsuk, F. Alessio and V. Pugatch, *LHC<sub>B</sub> RMS status and operation at 13 TeV*, in *Proceedings of the third French-Ukrainian workshop on the instrumentation developments for HEP*, pp. 61–65, 2015, <https://arxiv.org/abs/1512.07393> [[1512.07393](#)].
- [21] O. Okhrimenko, V. Iakovenko, V. Pugatch, F. Alessio and G. Corti, *The Radiation Monitoring System for the LHC<sub>B</sub> Inner Tracker*, *Conf. Proc.* **C111010** (2011) WEPMU024.
- [22] O.Y. Okhrimenko, V.M. Iakovenko and V.M. Pugatch, *The first LHC beam impact measured by the LHC<sub>B</sub> inner tracker radiation monitoring system*, in *3rd International Conference on Current Problems in Nuclear Physics and Atomic Energy*, pp. 639–643, 2011, <https://inspirehep.net/files/365654bcc7d8dff1f2bde7d3ed8dfec4>.

- [23] V. Pugatch, V.M. Aushev, V. Kyva, I. Kolomiets, Y.N. Pavlenko, S. Prystupa et al., *Radiation monitoring system for the LHCb Inner Tracker*, Tech. Rep. [LHCb-2002-067](#), [CERN-LHCb-2002-067](#), CERN, Geneva (2002).
- [24] V. Pugatch, K. Knöpfle and Y. Vassiliyev, *Beam profile imaging target*, *Nuclear Physics A* **701** (2002) 204.
- [25] V. Aushev et al., *Target monitoring system for HERA-B experiment. Multitarget operation*, *Nuclear Physics and Atomic Energy* **2** (2001) 56.
- [26] K. Riechmann, K. Knöpfle and V. Pugatch, *Pion and proton induced radiation damage to silicon detectors*, *Nucl. Instrum. and Methods in Phys. Res. A* **377** (1996) 276.
- [27] E.J. Sternglass, *Theory of Secondary Electron Emission by High-Speed Ions*, *Phys. Rev.* **108** (1957) 1.
- [28] H. Bruining, *Physics and Applications of Secondary Electron Emission: Electronics and Waves—a Series of Monographs*, Elsevier (2016).
- [29] STMicroelectronics, *Reference manual RM0090. STM32F405/415, STM32F407/417STM32F427/437 and STM32F429/439 advanced Arm-based 32-bit MCUs*, June, 2024.
- [30] LHCb collaboration, *LHCb online system, data acquisition and experiment control*, Technical design report. LHCb, CERN, Geneva (2001).
- [31] L. Cardoso, F. Alessio, J. Barbosa, P.-Y. Duval, C. Gaspar and R. Schwemmer, *A Framework for Hardware Integration in the LHCb Experiment Control System*, in *15th International Conference on Accelerator and Large Experimental Physics Control Systems*, p. MOPGF052, 2015, [DOI](#).
- [32] J. Barbosa, C. Gaspar, B. Jost, M. Frank and L.G. Cardoso, *A Monitoring System for the LHCb Data Flow*, *IEEE Trans. Nucl. Sci.* **64** (2017) 1191.
- [33] LHCb collaboration, *Precision luminosity measurements at LHCb*, *Journal of Instrumentation* **9** (2014) P12005 [[1410.0149](#)].
- [34] LHCb collaboration, *Absolute luminosity measurements with the LHCb detector at the LHC*, *Journal of Instrumentation* **7** (2012) P01010 [[1110.2866](#)].
- [35] S. van der Meer, *Calibration of the effective beam height in the ISR*, Tech. Rep. [CERN-ISR-PO-68-31](#), [ISR-PO-68-31](#), CERN, Geneva (1968).
- [36] V. Balagura, *Van der Meer scan luminosity measurement and beam–beam correction*, *Eur. Phys. J. C* **81** (2021) 26 [[2012.07752](#)].